SIAM J. SCI. COMPUT.
Vol. 41, No. 5, pp. S390–S408

A NONLINEAR ELIMINATION PRECONDITIONED INEXACT NEWTON METHOD FOR HETEROGENEOUS HYPERELASTICITY*

SHIHUA GONG† AND XIAO-CHUAN CAI‡

Abstract. We propose and study a nonlinear elimination preconditioned inexact Newton method for the numerical simulation of diseased human arteries with a heterogeneous hyperelastic model. We assume the artery is made of layers of distinct tissues and also contains plaque. Traditional Newton methods often work well for smooth and homogeneous arteries but suffer from slow or no convergence due to the heterogeneousness of diseased soft tissues when the material is quasi-incompressible. The proposed nonlinear elimination method adaptively finds a small number of equations causing the nonlinear stagnation and then eliminates them from the global nonlinear system. By using the theory of affine invariance of Newton method, we provide insight into why the nonlinear elimination method can improve the convergence of Newton iterations. Our numerical results show that the combination of nonlinear elimination with an initial guess interpolated from a coarse level solution can lead to the uniform convergence of Newton method for this class of very difficult nonlinear problems.

Key words. nonlinearly preconditioned Newton method, hyperelasticity, arterial walls, finite elements

AMS subject classifications. 65F08, 65N55, 65N22, 74S05

DOI. 10.1137/18M1194936

1. Introduction.

Nonlinearly preconditioned inexact Newton (IN) algorithms [7, 8, 14, 15] have been applied with significant success to solve difficult nonlinear problems in computational fluid dynamics involving boundary layers, local singularities, or shock waves. In this paper, we consider applying nonlinear preconditioning techniques to solve a heterogeneous hyperelastic problem arising from the modeling of diseased arteries. Arterial walls are composed of three distinct tissue layers from inside to outside: the intima, the media, and the adventitia. The mechanical properties of the intima can be negligible. The other two layers can be modeled as fiber-reinforced materials composed of a nearly incompressible matrix embedded with collagen fibers. For the disease of atherosclerosis, some plaque components of calcification and lipids may build up inside the arteries. In [6], the authors consider several material models for diseased arterial walls in order to study the mechanical response and the influence on the nonlinear iterations. It is reported that both the heterogeneousness of diseased soft tissues and the quasi-incompressibility have negative effects on the convergence of Newton method.

To accelerate the convergence of Newton iteration, nonlinear preconditioning is introduced as built-in machinery for the IN algorithm [9, 11] in order to deal with the unbalanced nonlinearities. It can be applied on the left or on the right of the nonlinear function. The additive Schwarz preconditioned inexact Newton algorithm (ASPIN)

*Received by the editors June 18, 2018; accepted for publication (in revised form) July 9, 2019; published electronically October 29, 2019.

https://doi.org/10.1137/18M1194936

Funding: The work of the first author was partially supported by National Natural Science Foundation of China 91430215. The work of the second author was partially supported by NSF DMS-1720366.

†Department of Mathematical Sciences, University of Bath, Bath BA2 7AY, UK (sg2328@bath.ac.uk).

‡Department of Computer Science, University of Colorado Boulder, Boulder, CO 80309 (cai@cs.colorado.edu).

[7] is an example of the left preconditioning and was observed in [7] to provide a more "balanced" system. On the other hand, right preconditioning techniques such as nonlinear elimination (NE) [8, 14, 15, 20] effectively modify the variables of the nonlinear system. NE is easier to implement than ASPIN since the nonlinear function does not have to be changed and the NE step does not have to be called at every outer Newton iteration. Moreover, more efficient and sophisticated linear solvers can be applied to the unchanged Jacobian.

An early work on NE is presented in [20], where the authors discussed how NE can retain the higher-order convergence of Newton method near the root of the system of nonlinear equations. It is still a nontrivial task to choose some subfunctions or variables to eliminate such that the convergence of Newton method becomes faster. For some computational fluid dynamics problems, the robustness and the effectiveness of NE are demonstrated in [14, 15]. Here NE is applied to those variables with high local nonlinearity as characterized by the local Lipschitz constant. The nonlinear FETI-DP (finite element tearing and interconnecting dual-primal) and BDDC (balancing domain decomposition by constraint) [16, 17, 18] domain decomposition methods also use the concept of NE and obtain satisfying parallel scalability using different NE strategies.

However, a straightforward application of NE to hyperelasticity does not work well probably because it introduces sharp jumps in the residual near the boundary of the eliminating subdomains. We refer to this as the thrashing phenomenon. Such jumps deteriorate the performance of nonlinear preconditioning. To resolve this problem, we use the theory of affine invariance [10] to analyze the convergence of the damped Newton method with exact NE, and then provide some insight into how to design the NE preconditioner. Our proposed algorithm is a two-level method with two key components: an adaptive NE scheme and a nodal-value interpolation operator. The interpolation operator provides an initial guess with a coarse level approximation to deal with the global nonlinearity. Note that for quasi-incompressible linear elasticity, the nodal interpolation is unstable since it does not preserve the volume. Thus, the IN method fails even with an initial guess interpolated from a coarse level solution, which is observed from our numerical experiments. Another reason for this may be due to the different geometry approximations by different level meshes for a curved domain. The interpolation may introduce local pollution to the initial guess. However, with the help of an adaptive NE scheme, we can capture the local pollution causing unbalanced nonlinearity and then eliminate it from the global system. We numerically show that this combination leads to a uniform convergence for Newton iterations.

The rest of the paper is organized as follows. We present the model and the discretization for arterial walls in section 2. The NE preconditioned Newton method is proposed and discussed in section 3. In section 4, some numerical experiments are presented to demonstrate the performance of the NE preconditioning. The concluding remarks are given in the last section.

2. Model and discretization. We consider a hyperelastic model for arterial walls and its finite element discretization. First, we introduce some basic notation in continuum mechanics. The body of interest in the reference configuration is denoted by $\Omega \in \mathbb{R}^3$, parameterized by X, and the current configuration by $\tilde{\Omega} \in \mathbb{R}^3$, parametrized by x. The deformation map $\phi(X) = X + u : \Omega \mapsto \tilde{\Omega}$ is a differential isomorphism between the reference and the current configuration. Here u is the displacement defined on the reference configuration. The deformation gradient $\boldsymbol{F}$ is defined by

$$\boldsymbol{F}(X) = \nabla\phi(X) = \boldsymbol{I} + \nabla u$$

with the Jacobian $J(X) = \det \boldsymbol{F}(X) > 0$. The right Cauchy–Green tensor is defined by

$$\boldsymbol{C} = \boldsymbol{F}^T\boldsymbol{F}.$$

The hyperelastic materials postulate the existence of an energy density function ψ defined per unit reference volume. By the principle of material frame indifference [19], one can prove that the energy function is a function of $\boldsymbol{C}$, i.e., $\psi = \hat{\psi}(\boldsymbol{C})$. Based on a specific form of the energy function, the first and second Piola–Kirchhoff stress tensors are

$$\boldsymbol{P} = \boldsymbol{F}\boldsymbol{S} \quad \text{and} \quad \boldsymbol{S} = 2\frac{\partial\psi}{\partial\boldsymbol{C}}.$$

And the Cauchy stress is given by $\boldsymbol{\sigma} = J^{-1}\boldsymbol{F}\boldsymbol{S}\boldsymbol{F}^T$. The balance of the momentum is governed by the hyperelastic equation

$$\begin{cases} -\mathrm{div}(\boldsymbol{F}\boldsymbol{S}) = f & \text{on} \quad \Omega, \\ u = \bar{u} & \text{on} \quad \Gamma_g, \\ \boldsymbol{P}N = \bar{t} & \text{on} \quad \Gamma_h, \end{cases} \tag{2.1}$$

where f is the body force vector, N denotes unit exterior normal to the boundary surface Γ_h, and $\partial\Omega = \Gamma_g \cup \Gamma_h$ with $\Gamma_g \cap \Gamma_h = \emptyset$. In the rest of the paper, we always consider homogeneous Dirichlet boundary condition $\bar{u} = 0$ and the situation where the deformation is driven by external applied pressure load. The simple pressure boundary condition is a distributed load normal to the applied surface in the reference configuration; it reads as $\bar{t} = -pN$. We are also interested in the follower pressure load [5], which is applied to the current deformed state; it reads as

$$\bar{t} = -p(\mathrm{cof}\boldsymbol{F})N.$$

Here $\mathrm{cof}\boldsymbol{F} = J\boldsymbol{F}^{-T}$ is the cofactor of $\boldsymbol{F}$. It concerns the change in direction of the normals as well as the area change. The dependence on the deformed geometry makes this a nonlinear boundary condition, which brings extra challenge for the convergence of the nonlinear solvers.

2.1. Energy functions for arterial walls with plaques. We are interested in a diseased artery with two layers and two plaque components. The schematic cross section of the artery is presented in Figure 2.1. There are a calcification and a lipid pool. The adventitia and the media are modeled by a polyconvex energy function [4]

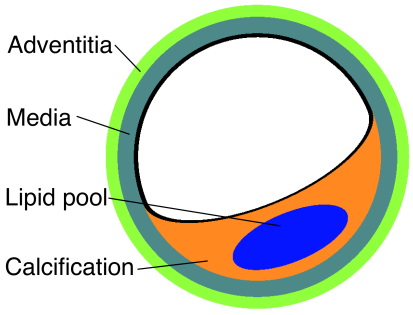

FIG. 2.1. *Schematic cross section of a diseased artery with two plaque components.*

$$\psi_A = c_1\left(\frac{I_1}{I_3^{1/3}} - 3\right) + \epsilon_1\left(I_3^{\epsilon_2} + \frac{1}{I_3^{\epsilon_2}} - 2\right) + \sum_{i=1}^{2}\alpha_1\left\langle I_1 J_4^{(i)} - J_5^{(i)} - 2\right\rangle^{\alpha_2}. \tag{2.2}$$

Here, $\langle b\rangle$ denotes the Macaulay brackets defined by $\langle b\rangle = (|b|+b)/2$, with $b \in R$. And I_1, I_2, I_3 are the principal invariants of $\boldsymbol{C}$, i.e.,

$$I_1 := \mathrm{tr}(\boldsymbol{C}), I_2 := \mathrm{tr}(\mathrm{cof}\boldsymbol{C}), I_3 := \det \boldsymbol{C}.$$

The additional mixed invariants $J_4^{(i)}, J_5^{(i)}$ characterize the anisotropic behavior of arterial wall and are defined as $J_4^{(i)} = \mathrm{tr}[\boldsymbol{C}\boldsymbol{M}^{(i)}], J_5^{(i)} := \mathrm{tr}[\boldsymbol{C}^2\boldsymbol{M}^{(i)}], i = 1:2$, where $\boldsymbol{M}^{(i)} := a^{(i)} \otimes a^{(i)}$ are the structural tensors with $a^{(i)}, i = 1, 2$, denoting the direction fields of the embedded collagen fibers. This is based on the fact that only weak interactions between the two fiber directions are observed; for further arguments, see [13]. The polyconvexity condition in the sense of [2] is the essential condition to ensure the existence of energy minimizers and the material stability.

Following [6], the lipid is modeled by the isotropic part of ψ_A used for the adventitia and media. The calcification area is modeled as an isotropic Mooney–Rivlin material with the following energy function:

$$\psi_C = \beta_1 I_1 + \eta_1 I_2 + \delta_1 I_3 - \delta_2 \ln I_3.$$

To obtain a stress-free state in the reference configuration, the parameter δ_2 has to satisfy $\delta_2 = \beta_1 + 2\eta_1 + \delta_1$. The model parameters of the above energy functions are listed in Table 2.1.

2.2. Finite element discretization. As reported in [3], the lowest-order Lagrange finite element with linear shape functions is not sufficient to provide a good approximation for the arterial wall stresses. We use the $\mathcal{P}_2$ Lagrange finite element to approximate the displacement. Let $V_0 \subset H^1(\Omega, \mathbb{R}^3)$ be the finite element space defined on Ω. The variational problem finds a solution $u \in V_0$ such that

$$a(u, v) := \int_\Omega \boldsymbol{F}\boldsymbol{S} : \nabla v \; dX + \int_{\Gamma_h} pJ\boldsymbol{F}^{-T}N \cdot v \; ds = \int_\Omega f \cdot v \; dX \quad \forall v \in V_0. \tag{2.3}$$

Here the subscript of V_0 indicates that the functions in V_0 vanish on Γ_g. Newton-type methods require the Jacobian form of $a(u, v)$, i.e.,

$$\begin{aligned} \delta a(u; \delta u, v) = &\int_\Omega \boldsymbol{F}^T\nabla\delta u : \mathbb{C} : \boldsymbol{F}^T\nabla v + \nabla\delta u\boldsymbol{S} : \nabla v \; dX \\ &+ \int_{\Gamma_h} pJ\left(\mathrm{tr}(\boldsymbol{F}^{-1}\nabla\delta u)I - \boldsymbol{F}^{-T}(\nabla\delta u)^T\right)\boldsymbol{F}^{-T}N \cdot v \; ds, \end{aligned} \tag{2.4}$$

where $\mathbb{C} = \frac{\partial \boldsymbol{S}}{\partial \boldsymbol{C}} = \frac{\partial^2\psi}{\partial \boldsymbol{C}\partial \boldsymbol{C}}$ is the material tangential moduli. An explicit formula to compute $\mathbb{C}$ for the general form of free energy can be found in [22]. The first term

TABLE 2.1
Model parameters [6] *of the energy functions.*

Comp.	c_1[kPa]	ϵ_1[kPa]	ϵ_2[-]	α_1[kPa]	α_2[-]	β_1[kPa]	η_1[kPa]	δ_1[kPa]	δ_2[kPa]
Adv.	6.6	23.9	10	1503.0	6.3	–	–	–	–
Med.	17.5	499.8	2.4	30001.9	5.1	–	–	–	–
Liq.	17.5	499.8	2.4	–	–	–	–	–	–
Cal.	–	–	–	–	–	80.0	250.0	2000.0	2580.0

on the right-hand side of (2.4) is corresponding to the material stiffness, while the second term is corresponding to the geometric stiffness and the last term arises due to the follower pressure load. In the section of numerical results, we also consider the case using the simpler pressure load.

3. Inexact Newton method with nonlinear elimination preconditioning. In this section, we first describe the motivation of nonlinear preconditioning based on an affine invariant convergence theorem of Newton-type methods. After that, we analyze the precondtioning effect of NE and then give a detailed description of the NE preconditioned inexact Newton method (NEPIN).

We rewrite (2.3) as a system of n equations

$$F(u^*) = 0, \tag{3.1}$$

where $F \in C^1(D), F : D \mapsto \mathrm{R}^n$ with an n by n Jacobian $J = F'(u)$ and $D \subset \mathrm{R}^n$ open and convex. Given an initial guess u^0 of a solution u^*, the damped Newton method finds a sequence of iterates $\{u^k\}$ computed through

$$F'\left(u^k\right) p^k = -F\left(u^k\right), \tag{3.2}$$

$$u^{k+1} = u^k + \lambda^k p^k, \quad \lambda^k \in (0, 1]. \tag{3.3}$$

Here p^k is the Newton direction and λ^k is a scalar determined by a monotonicity test such that

$$T(u^{k+1}) \leq \theta T\left(u^k\right), \tag{3.4}$$

where $\theta \in (0, 1)$ and $T(u)$ is a level function measuring how close u is to the solution u^*. In most cases, one sets $T(u) = \frac{1}{2}\|F(u)\|_2^2$. We use $\|\cdot\|$ to denote a generic norm and $\|\cdot\|_p$ for the ℓ^p-norm.

The convergence of $\{u^k\}$ to u^* is quadratic if the initial guess is close enough to the desired solution and $\lambda^k \to 1$. However, a good initial guess is generally unavailable and the monotonicity test (3.4) often results in a really small step length λ^k. This phenomenon is described rigorously in Theorem 3.1 under the framework of affine invariance [10] with a localized version of the affine contravariant Lipschitz condition. The first assumption of our analysis is given as follows.

Assumption 1. Assume the affine contravariant Lipschitz condition holds:

$$\left\| \left(F'(v) - F'(u)\right)(v - u)\right\| \leq \tilde{\omega}_F \|F'(u)(v - u)\|^2 \quad \text{for any } v, u \in D. \tag{3.5}$$

Here we call $\tilde{\omega}_F$ a global affine contravriant Lipschitz constant.

Let p be the Newton direction of F at u and set $v - u = \lambda p$ in (3.5) for any $\lambda \in (0, 1]$. Thus, for any $u \in D$ and $\lambda \in (0, 1]$, let $\omega_{F,u,\lambda}$ be the minimum constant such that

$$\left\| \left(F'(u + \lambda p) - F'(u)\right) p\right\| \leq \omega_{F,u,\lambda} \lambda \|F'(u)p\|^2. \tag{3.6}$$

Here we call $\omega_{F,u,\lambda}$ a local affine contravariant Lipschitz constant. We also denote $\omega_{F,u} = \sup_{\lambda \in (0,1]} \omega_{F,u,\lambda}$ and $\omega_F = \sup_{u \in D} \omega_{F,u}$. Note that $\omega_{F,u,\lambda} \leq \tilde{\omega}_F$ by Assumption 1. Thus, the supremums $\omega_{F,u}$ and ω_F taken over a set of values bounded from above are well defined.

THEOREM 3.1. *Let $F'(u)$ be nonsingular for all $u \in D$ and Assumption 1 holds. With the notation $h_k := \omega_{F,u^k}\|F(u^k)\|$, and $\lambda \in (0, \min(1, 2/h_k)]$, we have*

$$\|F(u^k + \lambda p^k)\| \le t_k(\lambda)\|F\left(u^k\right)\|, \tag{3.7}$$

where $t_k(\lambda) := 1 - \lambda + \frac{1}{2}\lambda^2 h_k$. Moreover, if $h_k < 2$, we have

$$\|F(u^k + p^k)\| \le \frac{1}{2}\omega_F\|F\left(u^k\right)\|^2. \tag{3.8}$$

Proof. The proof here is presented for completeness; see [10] for the original one. By applying the Newton–Leibniz formula and Assumption 1, we obtain the estimate (3.7):

$$\begin{aligned}
\left\|F\left(u^k + \lambda p^k\right)\right\| &= \left\|F\left(u^k\right) + \int_{t=0}^{\lambda} F'\left(u^k + tp\right) p \; dt\right\| \\
&= \left\|(1-\lambda)F\left(u^k\right) + \int_{t=0}^{\lambda} \left(F'\left(u^k + tp^k\right) - F'\left(u^k\right)\right) p^k \; dt\right\| \\
&\le \left\|(1-\lambda)F\left(u^k\right)\right\| + \int_{t=0}^{\lambda} t\omega_{F,u^k}\left\|F\left(u^k\right)\right\|^2 \; dt \\
&= \left(1 - \lambda + \frac{1}{2}\lambda^2 h_k\right)\|F\left(u^k\right)\|.
\end{aligned}$$

To get a reduction on the norm of residual, the step length should be chosen in the interval $(0, \min(1, 2/h_k)]$. Moreover, if $h_k < 2$, let $\lambda = 1$ and then we obtain the quadratic convergence (3.8). ∎

According to the theorem, the convergence is quadratic when $h_k < 2$. For $h_k \ge 2$, the optimal step size is $\bar{\lambda}^k := \frac{1}{h_k}$. And then the optimal reduction rate of the residual, i.e., the minimal value of $t_k(\lambda)$ in (3.7), is $\bar{t}_k := 1 - \frac{1}{2h_k}$. If h_k has a uniform upper bound for all k, then the convergence of the damped Newton iteration would be acceptable.

However, if there are some iterations for which h_k is too large, stagnation in the nonlinear iteration may occur. Our main objective is to introduce built-in machinery (nonlinear preconditioning) to prevent the stagnation. The nonlinear residual curve behaves in several different ways:

- *The estimate* (3.7) *is sharp*; see the blue curve in Figure 3.1. The feasible step size λ that satisfies the monotonicity test (3.4) should be very small, and our theoretical analysis applies well in such a situation.
- *The estimate* (3.7) *is not sharp*; see the red and green curves in Figure 3.1. For the green one, there is no stagnation. For the red one, stagnation occurs and we need to apply nonlinear preconditioning, but our analysis is not able to explain the performance of the algorithm.

Based on the above discussion, an intuitive idea to precondition Newton method (to prevent the stagnation) is to make the quantity

$$h_k := \omega_{F,u^k}\|F\left(u^k\right)\| \tag{3.9}$$

smaller. In the following, we transform the nonlinear function $F(u^k)$ to $\mathcal{F}(\tilde{u}^k)$ via NE. Under appropriate assumptions, we prove that the local affine contravariant Lipschitz constant $\omega_{\mathcal{F},\tilde{u}^k,\lambda}$ of $\mathcal{F}$ as well as the new residual $\|\mathcal{F}(\tilde{u}^k)\|$ is smaller than that of the original nonlinear function $F(u^k)$.

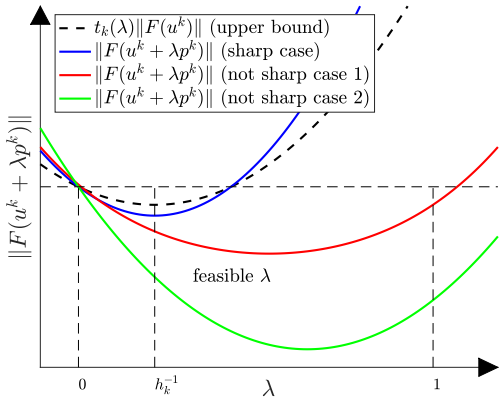

FIG. 3.1. *Possible residual curves for large h_k.*

3.1. Exact nonlinear elimination. Assume $F(u)$ is partitioned as

$$F(u) = \begin{bmatrix} F_1(u_1, u_2) \\ F_2(u_1, u_2) \end{bmatrix}, \tag{3.10}$$

and $u = (u_1, u_2)$. The Jacobian is partitioned accordingly as

$$J := F'(u) = \begin{bmatrix} J_{11} & J_{12} \\ J_{21} & J_{22} \end{bmatrix}, \tag{3.11}$$

where $J_{ij} = \frac{\partial F_i}{\partial u_j}$. We make the following assumption for the partition, with which the preconditioning effect is proved.

Assumption 2. For all $u \in D$ and all the considered partitions in (3.10), it holds that

1. $J_{11}(u)$ is nonsingular;
2. $\|J_{21}(u)J_{11}^{-1}(u)\|_1 \le 1$.

Remark 1. The first condition in Assumption 2 is essential to ensure the solvability of the subproblem $F_1(u_1, u_2) = 0$ for any fixed u_2. The second condition asserts a strong upper bound for $J_{21}(u)J_{11}^{-1}(u)$ in a certain norm. It is equivalent to

$$\|J_{11}v_1\|_1 \ge \|J_{21}v_1\|_1$$

for every v_1 with the same dimension of u_1. If we restrict the dimension of u_1 to 1, it is exactly the diagonally dominant property of a matrix. The ramification of this condition does not affect the computability of the NE algorithm but may lead to the residual oscillation during the iterations. Actually, the estimate (3.17) below still holds with an extra constant, namely

$$\|\mathcal{F}(u_2)\| \le \max(1, \|J_{21}J_{11}^{-1}\|_1)\|F(u_1, u_2)\|,$$

which indicates that the oscillation of the residual is stable. In order to obtain a better estimate, we assume $\|J_{21}J_{11}^{-1}\|_1 \le 1$, which is similar to the proof of the convergence of the Jacobi and Gauss–Seidel methods for diagonally dominant linear systems of equations.

Since J_{11} is nonsingular, for any u_2 in a projection set $D_2 = \{u_2 \mid (u_1, u_2) \in D\}$, there is an implicitly defined function $g(u_2)$ such that

$$F_1(g(u_2), u_2) = 0. \tag{3.12}$$

Then our preconditioned nonlinear problem reads as follows: find u_2 such that

$$\mathcal{F}(u_2) := F_2(g(u_2), u_2) = 0. \tag{3.13}$$

We call $\bar{u} = (g(u_2), u_2)$ as the *cut-extension* of u_2. Next, we analyze the convergence of the Newton method applied to the preconditioned system.

To derive the Jacobian of $\mathcal{F}$, one can first take the derivative of (3.12) with respect to u_2 and then have $J_{11}g'(u_2) + J_{12} = 0$. Since J_{11} is nonsingular, we have

$$g'(u_2) = -J_{11}^{-1}J_{12}. \tag{3.14}$$

Then, by differentiating (3.13) and using (3.14), we have

$$\mathcal{J}(u_2) := \mathcal{F}'(u_2) = \left(J_{22} - J_{21}J_{11}^{-1}J_{12}\right)(g(u_2), u_2). \tag{3.15}$$

Note that $\mathcal{J}(u_2)$ is the Schur complement of $J(\bar{u})$, where $\bar{u} = (g(u_2), u_2)$ is the cut-extension of u_2. Let $p_2 := -\mathcal{J}^{-1}(u_2)\mathcal{F}(u_2)$ be the Newton direction of $\mathcal{F}$. We define a harmonic extension of p_2 by $p = (h(p_2), p_2)$ such that $h(p_2)$ satisfies

$$J_{11}(\bar{u})h(p_2) + J_{12}(\bar{u})p_2 = 0,$$

or equivalently $h(p_2) = g'(u_2)p_2$. Thus, we have the linear approximation property

$$g(u_2 + \lambda p_2) \approx g(u_2) + g'(u_2)\lambda p_2 = g(u_2) + \lambda h(p_2)$$

for sufficiently small λ.

Moreover, one can show that p actually is the Newton direction of F at $\bar{u}$ since

$$J(\bar{u})p = \begin{bmatrix} J_{11} & J_{12} \\ J_{21} & J_{22} \end{bmatrix} \begin{bmatrix} h(p_2) \\ p_2 \end{bmatrix} = \begin{bmatrix} 0 \\ \mathcal{J}(u_2)p_2 \end{bmatrix} = \begin{bmatrix} -F_1\left(g(u_2), u_2\right) \\ -F_2\left(g(u_2), u_2\right) \end{bmatrix} = -F(\bar{u}). \tag{3.16}$$

Thus, we can obtain the precondtioned Newton direction p_2 directly by solving the original Jacobian system $J(\bar{u})p = -F(\bar{u})$ without assembling the Schur complement $\mathcal{J}(u_2)$.

LEMMA 3.2. *If Assumption* 2 *holds, then for any* $u = (u_1, u_2) \in D$, *we have*

$$\|\mathcal{F}(u_2)\|_1 \le \|F_2(u_1, u_2)\|_1 + \|J_{21}J_{11}^{-1}\|_1\|F_1(u_1, u_2)\|_1 \le \|F(u_1, u_2)\|_1. \tag{3.17}$$

Proof. By the Taylor expansion, we have

$$\begin{bmatrix} F_1(g(u_2), u_2) \\ F_2(g(u_2), u_2) \end{bmatrix} = \begin{bmatrix} F_1(u_1, u_2) \\ F_2(u_1, u_2) \end{bmatrix} + \begin{bmatrix} J_{11}(u_1^\theta, u_2)(g(u_2) - u_1) \\ J_{21}(u_1^\theta, u_2)(g(u_2) - u_1) \end{bmatrix},$$

where $u_1^\theta, u_1, g(u_2)$ are colinear. Since $F_1(g(u_2), u_2) = 0$ and J_{11} is nonsingular, we have $g(u_2) - u_1 = -J_{11}^{-1}F_1(u_1, u_2)$. Thus,

$$\mathcal{F}(u_2) = F_2(u_1, u_2) - (J_{21}J_{11}^{-1})(u_1^\theta, u_2)F_1(u_1, u_2).$$

By Assumption 2, we have $\|J_{21}J_{11}^{-1}\|_1 \le 1$. Thus, (3.17) follows from the triangle inequality

$$\|\mathcal{F}(u_2)\|_1 \le \|F_2(u_1, u_2)\|_1 + \|J_{21}J_{11}^{-1}F_1(u_1, u_2)\|_1 \le \|F(u_1, u_2)\|_1. \qquad \square$$

LEMMA 3.3. *If Assumption 2 holds, then for any $u_2 \in D_2$, we have*

$$\frac{\|(\mathcal{J}(u_2+\lambda p_2)-\mathcal{J}(u_2))p_2\|_1}{\lambda\|\mathcal{J}(u_2)p_2\|_1^2} \le \frac{\|\left(J(\bar{v})-J(\bar{u})\right)p\|_1}{\lambda\|J(\bar{u})p\|_1^2}. \tag{3.18}$$

Here $p_2 := -\mathcal{J}^{-1}(u_2)\mathcal{F}(u_2)$ and $p := -J^{-1}(\bar{u})F(\bar{u})$ are the Newton directions of $\mathcal{F}$ and F, respectively. And $\bar{u} := (g(u_2), u_2)$ and $\bar{v} := (g(u_2+\lambda p_2), u_2+\lambda p_2)$ are the cut-extension of u_2 and $u_2+\lambda p_2$, respectively.

Proof. By (3.16), we have

$$\|\mathcal{J}(u_2)p_2\|_1 = \|J^{\bar{u}}p\|_1. \tag{3.19}$$

Here we use the superscript $\bar{u}$ to indicate that the Jacobian is evaluated at $\bar{u}$, i.e., $J^{\bar{u}} = J(g(u_2), u_2)$. Set $\bar{v} = (g(u_2+\lambda p_2), u_2+\lambda p_2)$ and $v_2 = u_2+\lambda p_2$. We have

$$\begin{aligned}
\|\left(J^{\bar{v}}-J^{\bar{u}}\right)p\|_1 &= \left\| \begin{bmatrix} J_{11}^{\bar{v}}h(p_2)+J_{12}^{\bar{v}}p_2 \\ J_{21}^{\bar{v}}h(p_2)+J_{22}^{\bar{v}}p_2 \end{bmatrix} - \begin{bmatrix} 0 \\ \mathcal{J}(u_2)p_2 \end{bmatrix} \right\|_1 \\
&= \left\| \begin{bmatrix} \left(-J_{11}^{\bar{v}}(J_{11}^{\bar{u}})^{-1}J_{12}^{\bar{u}}+J_{12}^{\bar{v}}\right)p_2 \\ \left(-J_{21}^{\bar{v}}(J_{11}^{\bar{u}})^{-1}J_{12}^{\bar{u}}+J_{22}^{\bar{v}}\right)p_2 \end{bmatrix} - \begin{bmatrix} 0 \\ \mathcal{J}(u_2)p_2 \end{bmatrix} \right\|_1 \\
&= \left\| \begin{bmatrix} \tilde{J}_{12}p_2 \\ J_{21}^{\bar{v}}(J_{11}^{\bar{v}})^{-1}\tilde{J}_{12}p_2 \end{bmatrix} + \begin{bmatrix} 0 \\ \left(\mathcal{J}(v_2)-\mathcal{J}(u_2)\right)p_2 \end{bmatrix} \right\|_1 \\
&= \|\tilde{J}_{12}p_2\|_1 + \|J_{21}^{\bar{v}}(J_{11}^{\bar{v}})^{-1}\tilde{J}_{12}p_2 + \left(\mathcal{J}(v_2)-\mathcal{J}(u_2)\right)p_2\|_1 \\
&\ge \|\left(\mathcal{J}(v_2)-\mathcal{J}(u_2)\right)p_2\|_1 + \left(1-\|J_{21}^{\bar{v}}(J_{11}^{\bar{v}})^{-1}\|_1\right)\|\tilde{J}_{12}p_2\|_1,
\end{aligned} \tag{3.20}$$

where $\tilde{J}_{12} = -J_{11}^{\bar{v}}(J_{11}^{\bar{u}})^{-1}J_{12}^{\bar{u}} + J_{12}^{\bar{v}}$. Assumption 2 asserts $1-\|J_{21}^{\bar{v}}(J_{11}^{\bar{v}})^{-1}\|_1 \ge 0$. Thus,

$$\|\left(\mathcal{J}(u_2+\lambda p_2)-\mathcal{J}(u_2)\right)p_2\|_1 \le \|\left(J^{\bar{v}}-J^{\bar{u}}\right)p\|_1. \tag{3.21}$$

By (3.19) and (3.21), we complete the proof. ∎

The analysis provides us some insight about how to design the NE preconditioner:

1. *The nonlinear preconditioning effect.* The convergence of Newton-type methods relies on a certain form of Lipschitz condition. In (3.18) of Lemma 3.3, the left-hand side is a characterization of the affine contravariant Lipschitz constant of $\mathcal{F}$, whereas, for the right-hand side of F, it is not valid since the cut-extension

$$\bar{v} := \begin{pmatrix} g(u_2+\lambda p_2) \\ u_2+\lambda p_2 \end{pmatrix} \ne \bar{u}+\lambda p = \begin{pmatrix} g(u_2)+\lambda h(p_2) \\ u_2+\lambda p_2 \end{pmatrix}.$$

However, we have $g(u_2+\lambda p_2) = g(u_2)+\lambda h(p_2)+\mathcal{O}(\lambda^2)$ and then $\bar{v} \approx \bar{u}+\lambda p$. Thus, let F be sufficiently smooth and by Lemma 3.3 we obtain, for small λ and in the sense of ℓ^1-norm,

$$\omega_{\mathcal{F},u_2,\lambda} \le \omega_{F,\bar{u},\lambda} + \mathcal{O}(\lambda).$$

If the stagnation in the nonlinear residual appears, Theorem 3.1 tells us that the optimal step length $\bar{\lambda}^k = \frac{1}{h_k}$ should be really small. In such situations, the NE elimination accelerates the convergence of the Newton iteration by making the residual and the local affine contravariant Lipschitz constant smaller.

2. *How to perform NE*? To apply a Newton step to the nonlinear elimination preconditioned system (3.13), one requires a solve of the Schur complement system

$$\mathcal{J}p_2 = \mathcal{F}$$

and several solves of $g(u_2 + \lambda p_2)$ during the line search step to satisfy

$$\|\mathcal{F}(g(u_2 + \lambda p_2), u_2 + \lambda p_2)\| \leq \theta \|\mathcal{F}(g(u_2), u_2)\|.$$

This is often considered too expensive in realistic applications. Fortunately, according to our analysis, we can obtain the precondtioned Newton direction p_2 directly by solving the original Jacobian system

$$J(\bar{u})p = -F(\bar{u}),$$

provided that $F_1(\bar{u}) = F_1(g(u_2), u_2) = 0$. And then we have $p = (h(p_2), p_2)$. Moreover, we have the approximation $(g(u_2 + \lambda p_2), u_2 + \lambda p_2) \approx \bar{u} + \lambda p$. Thus, the line search can be carried out approximately as

$$\|F(\bar{u} + \lambda p)\| \leq \theta \|F(\bar{u})\|.$$

From this point of view, the NE preconditioner only needs to update the approximate solution $u = (u_1, u_2)$ to $\bar{u} = (g(u_2), u_2)$ before each Newton iteration of the original problem, and the implementation of the Newton iteration does not change, including assembling the Jacobian matrix and assembling the residual vector and the linear solver.

3. *How to choose the eliminated equations*? According to Lemma 3.2, the reduction rate on the residual is bounded by

$$\frac{\|F_2\|_1 + \|J_{21}J_{11}^{-1}\|_1 \|F_1\|_1}{\|F\|_1}.$$

Note that the subscripts in F_1, F_2, J_{11}, and J_{21} correspond to a partition of the nonlinear functions and variables. Assumption 2 ensures that there exists a uniform upper bound for $\|J_{21}J_{11}^{-1}\|_1$ with respect to all partitions under consideration. If the upper bound for $\|J_{21}J_{11}^{-1}\|_1$ is strictly smaller than 1, one should choose F_1 to be as large as possible such that these values are reduced through a multiplication with $\|J_{21}J_{11}^{-1}\|_1$.

4. *How to choose the eliminated variables*? Assumption 2 asserts $\|J_{21}J_{11}^{-1}\|_1 \leq 1$. A weaker requirement is

$$\|J_{21}(u)\|_1 \leq \|J_{11}(u)\|_1.$$

For some elliptic problems, it is usually satisfied due to the diagonally dominant property. In the cases of the finite element discretization, each equation is associated with a basis function and the variables are the coefficients of the solution. To maximize the norm $\|J_{11}(u)\|_1$, one should choose the eliminated variables such that the eliminated equations and the eliminated variables are associated with the same finite element basis functions. For the saddle-point problems, we should use some point-block strategies, which means we group all physical components associated with a mesh point as a block and always perform elimination for this small block. This paper does not cover the point-block strategies; please see [14] for more details.

3.2. Inexact nonlinear elimination. In this subsection, we first present a basic nonlinear solver: an IN method [9, 11]. After that, we propose a nonlinearity checking scheme to detect the eliminated equations and then embed the NE preconditioner into IN, which is briefly described here. Suppose u^k is the current approximate solution; a new approximate solution u^{k+1} is computed through the following two steps

ALGORITHM 1 (IN).
Step 1. *Find the IN direction* p^k *such that*

$$\|F\left(u^k\right) + F'(u^k)p^k\| \leq \max(\eta_a, \eta_r \|F\left(u^k\right)\|).$$

Step 2. *Compute the new approximate solution with suitable damping coefficient* λ^k

$$u^{k+1} = u^k + \lambda^k p^k.$$

Here η_a and $\eta_r \in [0, 1)$ are the absolute and relative tolerances that determine how accurately the Jacobian system needs to be solved, and λ^k is another scalar that determines how far one should go in the selected direction.

3.2.1. Nonlinearity checking and subproblem construction. As discussed following the proof of Theorem 3.1, the nonlinear preconditioning is introduced to prevent stagnation in the nonlinear iteration. Thus, before performing NE, we need to evaluate the local nonlinearity of the nonlinear function. We use the following criterion for the nonlinearity checking:

$$\frac{\|F\left(u^k\right)\|}{\|F(u^{k-1})\|} \leq \rho_{rdt},$$

where $\rho_{rdt} \in (0, 1)$ is a prechosen tolerance. If the reduction rate in the residual is smaller than ρ_{rdt}, the global IN iteration works well and the NE is not needed. Otherwise, we perform NE.

NE substitutes the current guess u^k by $\bar{u}^k$, which is obtained by solving a nonlinear subproblem. Next we construct the subproblem in an algebraic way. Let n be the size of the global nonlinear problem and

$$S = \{1, \ldots, n\}$$

be the global index set, i.e., one integer for each unknown u_i and the corresponding F_i. Note that, different from the subscripts in section 3.1, here we abuse the notation of the subscript to indicate a component of the vectors or the degree of freedom. The following index set collects the degrees of freedom with large residual components (which we call bad components):

$$S_b := \{j \in S \mid |F_j\left(u^k\right)| > \rho_{res} \|F\left(u^k\right)\|_\infty\}.$$

Here $\|F(u^k)\|_\infty = \max_{i=1}^n |F_i(u^k)|$ is the infinity norm taken over the global index set S and $\rho_{res} \in (0, 1)$ is a prechosen tolerance.

According to our numerical tests, sharp jumps in the residual function would be introduced if we only eliminate the equations and variables with indices in S_b. A trick to prevent these jumps is to extend S_b to S_b^δ by adding the degrees of freedom with overlapping δ to S_b. Here the overlapping δ is an integer corresponding to the

connectivity in the graph characterized by the global Jacobian matrix. Thus, the resulting subspace is denoted by

$$V_b^\delta = \{v \mid v = (v_1, \ldots, v_n)^T \in \mathrm{R}^n, v_i = 0, \text{ if } i \notin S_b^\delta\}.$$

The corresponding restriction matrix is denoted by $R_b^\delta \in \mathrm{R}^{n\times n}$, whose ith column is either zero if $i \notin S_b^\delta$ or the ith column of the indentity matrix $I_{n\times n}$.

Given an approximate solution u^k and an index set S_b^δ, the NE algorithm finds the correction by approximately solving $u_b^\delta \in V_b^\delta$,

$$F_b^\delta(u_b^\delta) := R_b^\delta F(u_b^\delta + u^k) = 0. \tag{3.22}$$

The new approximate solution is obtained as $\bar{u}^k = u_b^\delta + u^k$. It is easy to see that the Jacobian of (3.22) is $J_b^\delta(u_b^\delta) = R_b^\delta J(u_b^\delta + u)(R_b^\delta)^T$, where $J = F' = (\frac{\partial F_i}{\partial u_j})_{n\times n}$.

Before performing NE, we need to estimate the computational cost for solving the subproblem (3.22). If the size of the subproblem is too large, it indicates that the residual is large in most of the domain and the current approximate solution is really bad. We need to find a better initial guess or perform the global inexact Newton iteration in such a situation. If the condition

$$\#(S_b^\delta) < \rho_{size} n$$

is satisfied, we solve the subproblem (3.22) approximately such that

$$\|F_b^\delta(u_b^\delta)\| \le \max(\gamma_a, \gamma_r \|R_b^\delta F\left(u^k\right)\|).$$

Here ρ_{size} is the tolerance to limit the size of the subproblem and γ_a, γ_r are the absolute and relative tolerances on how accurately the subproblem needs to be solved. We list all the algorithm parameters related to the NE in Table 3.1.

3.2.2. Preconditioned algorithm. We summarize the NEPIN: Given an initial guess u^0 (zero or interpolated from a coarse level solution), a sequence of approximate solution $\{u^k\}$ is computed as follows.

ALGORITHM 2 (NEPIN).

Step 1. *Perform the nonlinearity checking:*

1.1. *If the reduction rate* $\frac{\|F(u^k)\|}{\|F(\bar{u}^{k-1})\|} \le \rho_{rdt}$, *set* $\bar{u}^k = u^k$ *and go to Step* 3.

1.2. *Find the eliminated degrees of freedom and construct the index set* S_b^δ.

1.3. *If* $\#(S_b^\delta) < \rho_{size} n$, *go to Step* 2. *Otherwise, set* $\bar{u}^k = u^k$ *and go to Step* 3.

TABLE 3.1
A list of parameters needed in NE.

NE parameters	Description
ρ_{rdt}	A tolerance to evaluate the local nonlinearity. If the reduction rate of the residual is smaller than ρ_{rdt}, we skip NE.
ρ_{res}	A tolerance to determine how large a residual component should be for elimination.
δ	An integer to enrich the eliminating index set S_b.
ρ_{size}	A tolerance to restrict the size of the subproblem.
γ_a	An absolute tolerance on how accurately the subproblem should be solved.
γ_r	A relative tolerance on how accurately the subproblem should be solved.

Step 2. *Compute the correction* $u_b^\delta \in V_b^\delta$ *by solving the subproblem approximately*

$$F_b^\delta(u_b^\delta) := R_b^\delta F\left(u_b^\delta + u^k\right) = 0$$

with a tolerance $\text{tol} = \max(\gamma_a, \gamma_r \|R_b^\delta F(u^k)\|)$. *If* $\|F(u_b^\delta + u^k)\| < \|F(u^k)\|$, *accept the correction and update* $\bar{u}^k \leftarrow u_b^\delta + u^k$. *Go to Step* 3.

Step 3. *Compute the new approximate solution* u^{k+1} *by one step of IN for the original nonlinear problem*

$$F(u) = 0$$

with the current guess $\bar{u}^k$. *If the global convergent condition is satisfied, stop. Otherwise, go to Step* 1.

In an NE step, we only accept the correction by NE if the resulting residual norm is smaller. This is based on Lemma 3.2, which tells us that an effective NE should reduce the global residual. This requirement actually is very strong. However, according to our numerical tests, it can be satisfied if a good initial guess is provided or the tolerance δ is appropriately set.

3.2.3. Parallelization and global algebraic solvers. The index set S_b^δ for the bad components is constructed in a purely algebraic fashion. And the NE step described in previous sections is carried out on the whole domain. For the purpose of parallel computing, we decompose the domain into nonoverlapping subdomains $\Omega = \cup_{l=1}^N \bar{\Omega}_l$ and construct index sets of bad components on every subdomain. The NE on the subdomains can be carried out in parallel. Moreover, the parallel iterative linear solver with restricted additive Schwarz (RAS) preconditioner is implemented based on the same data layout.

First we discuss the parallelization of NE in detail. We assume that $S_1, \ldots, S_N$ is a nonoverlapping partition of S in the sense that

$$S = \cup_{i=l}^N S_l, \quad S_l \cap S_k = \emptyset \text{ if } l \neq k.$$

One can form the index set S_i by collecting all the degrees of freedom located in subdomain Ω_i. The index sets corresponding to the bad components are defined as

$$S_{b,l} = S_b \cap S_l = \{j \in S_l \mid |F_j\left(u^k\right)| > \rho_{res} \|F\left(u^k\right)\|_\infty\}, l = 1 : N.$$

Note that the subscript b is an abbreviation of "bad," while l is the index for the subdomain. The selection procedure of $S_{b,l}$ is carried out locally on subdomain Ω_l, but the threshold $\|F(u^k)\|_\infty$ is evaluated globally on all processors. The extension from $S_{b,l}$ to $S_{b,l}^\delta$ is by adding the degrees of freedom with an algebraic distant δ to $S_{b,l}$. Thus, $S_{b,l}^\delta$ may contain some ghost indices, which belong to other processors. We can then define the local spaces of bad components similarly as

$$V_{b,l}^\delta = \{v \mid v = (v_1, \ldots, v_n)^T \in \mathrm{R}^n, v_i = 0, \text{ if } i \notin S_{b,l}^\delta\},$$

as well as the corresponding restriction (also prolongation) matrix $R_{b,l}^\delta$. The subproblem on each subdomain is to approximately find $u_{b,l}^\delta \in V_{b,l}^\delta$ such that

$$F_{b,l}^\delta(u_{b,l}^\delta) := R_{b,l}^\delta F\left(u_{b,l}^\delta + u^k\right) = 0$$

with zero initial guess. In the situation of parallel computing, we do not restrict the size of the subproblems. The parallel NE step is ended by a restricted update for the approximate solution

$$\bar{u}^k \leftarrow u^k + \sum_{l=1}^{N} R_{b,l}^0 u_{b,l}^{\delta}.$$

Note that we accept the update only if the global residual $\|F(\bar{u}^k)\|$ is smaller than $\|F(\bar{u}^k)\|$.

Second, we discuss some basic components of the global algebraic solvers. Both the IN and NEPIN algorithms involve a global Newton iteration, for which we always use the same global settings. The stopping criterion for the global Newton iterations is

$$\|F\left(u^k\right)\| \leq \max(1\text{e}{-10}, 1\text{e}{-6}\|F(u^0)\|).$$

The backtracking line search strategy is used to determine the maximum step length to move along the approximate Newton direction. For solving the global Jacobian systems, we use the right-preconditioned GMRES with zero initial guess and the restart is set to 200. The stopping criterion for the linear solver is

$$\|F\left(u^k\right) + F'(u^k)p^k\| \leq \max(1\text{e}{-10}, 1\text{e}{-5}\|F\left(u^k\right)\|).$$

The RAS preconditioner is implemented based on the same data layout as the NE elimination. Corresponding to the partition $S = \cup_{l=1}^{N} S_l$, we denote the local spaces by V_l and the local restriction (also prolongation) by $R_l^{\tilde{\delta}}$. Thus, the RAS preconditioner can be written as

$$B^k = \sum_l R_l^0 (A_l^{k,\tilde{\delta}})^{-1} R_l^{\tilde{\delta}},$$

where $A_l^{k,\tilde{\delta}} = R_l^{\tilde{\delta}} J^k R_l^{\tilde{\delta}}$. We set the overlap as $\tilde{\delta} = 3$ and use LU factorization to solve the subdomain problems. There are many other choices for the linear solver and the linear preconditioner. Since the focus of the paper is on the nonlinear solver, we don't exploit the other possibilities related to the linear problems.

4. Numerical results and discussion. In this section, we present some numerical results for solving the nonlinear variational problem (2.3). Our three-dimensional geometry is built through extruding the cross section in Figure 2.1 by 2mm. We assume the inner radius of the artery is 1cm. The thickness of the media and adventitia layers is 1.32mm and 0.96mm (see [12]), whereas the mean thickness of the plaques of lipid pool and calcification are 3mm and 2mm. A pressure of up to 24kPa ($\approx$ 180mmHg) is applied to the interior of the arterial segment, which is the upper range of the physiological blood pressure. The discretization for hyperelasticity and the nonlinear solvers described in the previous sections are implemented by using FEniCS [21] and PETSc [1], respectively.

We first validate our algorithm and implementation. Then we compare the performance of the classical IN method with our new algorithm. In the end, we discuss the robustness of NE.

4.1. Validation of algorithm and software. It is hard to construct an analytic solution for the nonlinear variational problems. One way to validate the result is to observe the mesh convergence of the numerical solutions. We generate four tetrahedral meshes for the arterial segment, denoted M_1, M_2, M_3, and M_4. The degrees of freedom defined on these meshes are 10080, 21693, 101046, and 653601, respectively. Because of the curved boundary of the artery, the domains occupied by these meshes are a little bit different. We plot the numerical solutions of displacement in Figure 4.1

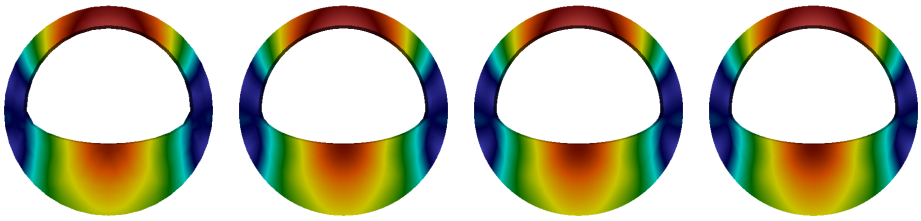

FIG. 4.1. *Numerical solutions of the displacement corresponding to meshes M_1, M_2, M_3, M_4 from left to right (simple boundary load).*

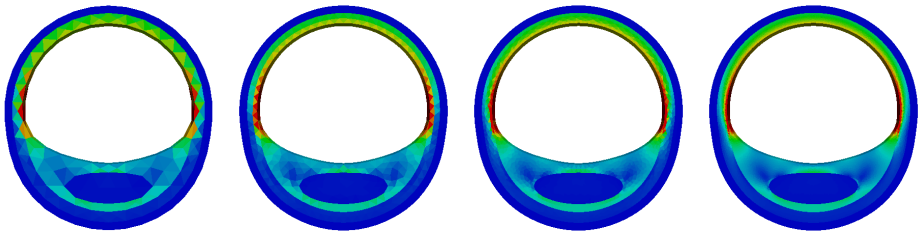

FIG. 4.2. *von Mises stresses on the deformed configurations corresponding to meshes M_1, M_2, M_3, M_4 from left to right (follower boundary load).*

TABLE 4.1
Errors of numerical solutions: $\bar{e} = I_{h_i}^{h_4}\bar{u}_{h_i} - \bar{u}_{h_4}$, $e_i = I_{h_i}^{h_4}u_{h_i} - u_{h_4}$, and d_{alg} stands for the difference of numerical solutions obtained by IN and NEPIN.

	Simple pressure load				Follower pressure load			
Mesh	$\|d_{alg}\|_0$	$\|d_{alg}\|_1$	$\|\bar{e}_i\|_0$	$\|\bar{e}_i\|_1$	$\|d_{alg}\|_0$	$\|d_{alg}\|_1$	$\|e_i\|_0$	$\|e_i\|_1$
M_1	2.63e−07	2.72e−09	0.294	0.617	4.48e−10	7.23e−11	0.247	0.698
M_2	4.23e−10	4.96e−11	0.147	0.401	1.99e−9	1.52e−9	0.175	0.449
M_3	3.04e−9	3.62e−10	0.071	0.234	1.95e−7	1.28e−6	0.089	0.274

for the case of the simple boundary load and the von Mises stresses in Figure 4.2 for the case of follower boundary load. The deformation driven by the simple pressure load is bigger than that driven by the follower pressure load, but their distributions and the stresses are similar.

We compute the difference of the numerical solutions obtained by IN and NEPIN; see Table 4.1. They are almost identical. We also consider the actual measurements of the solution error by taking the numerical solution on the finest mesh as a reference solution and interpolating the coarse level solutions into the finest mesh. Table 4.1 lists the errors in L^2- and H^1-norms. We denote by $\bar{u}_{h_i}$ the numerical solution on M_i driven by the simple pressure load and by u_{h_i} that driven by the follower pressure load. We also denote the nodal interpolation operator by $I_{h_i}^{h_j}$, which prolongates the numerical solutions from M_i to M_j. Note that some nodal values are computed via extrapolation since these nodes of the fine mesh are outside the domain occupied by the coarse mesh. We cannot compute the convergence orders since the meshes are not quasi-uniform. But it is still clear that the computed solutions converge as the mesh size goes to zero.

4.2. A comparison of IN and NEPIN. To get the best performance of NEPIN, we try various settings of the parameters needed in NE and eventually

TABLE 4.2
Settings for the parameters needed in NE.

Mesh	ρ_{rdt}	ρ_{res}	δ	ρ_{size}	γ_a	γ_r
M_1	0.7	0.9	0	5%	1e−6	1e−1
M_2	0.7	0.9	0	5%	1e−6	1e−1
M_3	0.7	0.8	1	5%	1e−6	1e−1
M_4	0.7	0.8	2	5%	1e−6	1e−1

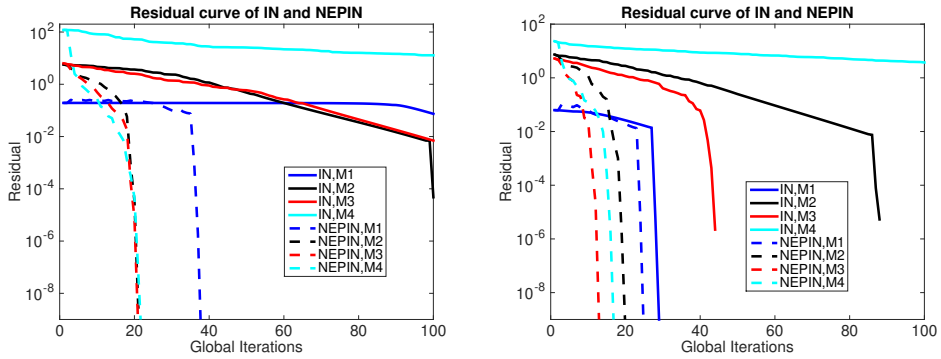

FIG. 4.3. *Histories of IN and NEPIN (left: simple pressure load; right: follower pressure load).*

recommend using the settings in Table 4.2. Figure 4.3 shows the histories of the residual of IN and NEPIN starting from the best available initial guesses. Namely, the initial guess for M_i is interpolated from the numerical solution of M_{i-1}. The convergence of NEPIN is almost uniform for all meshes if the initial guesses are interpolated from a coarse level approximation. For the coarsest grid, the result is not as good as others. But NE still improves the convergence a little bit in this case. In the context of quasi-incompressible linear elasticity, the nodal interpolation is unstable since it does not preserve the volume. Note that the change of material volume induces a large residual due to the volumetric term in the hyperelastic energy. But in our numerical tests for quasi-incompressible hyperelasticity, the combination of NE with the nodal interpolation works well.

We also use different initial guesses to compare the performance of IN and NEPIN. The numbers of global Newton iterations are summarized in Tables 4.3–4.4. The letter F indicates that the iteration does not converge in 200 steps. The first thing we observe from Tables 4.3–4.4 is that NEPIN always converges faster than IN while using the same initial guess and the same mesh. For the zero initial guess, the performance of NE is not good enough. Actually, both methods with zero initial guess fail in the case of the follower load. If an initial guess is too far from the solution, the local NE does not help much for the global Newton iteration. However, once an approximate initial guess is provided, the performance of nonlinear elimination is prominent. Note that IN with the same initial guess still suffers from slow convergence.

4.3. The effect of the tolerances in NEPIN. It is unfair to directly compare the total number of global nonlinear iterations of IN and NEPIN, since NEPIN has another Newton iteration wrapped inside. In this subsection, we expose the detail of the inner Newton iteration of NEPIN. We set $\rho_{rdt} = 0.7$ to evaluate the local nonlinearity and set $\rho_{size} = 5\%$ to limit the subproblem size. There are two main

TABLE 4.3
The number of global Newton iterations with different initial guesses (simple pressure load).

Method	IN				NEPIN			
Initial guess\mesh	M_1	M_2	M_3	M_4	M_1	M_2	M_3	M_4
0	104	121	109	93	38	49	58	92
$I_{h_1}^{h_i}\bar{u}_{h_1}$		100	94	F		21	24	F
$I_{h_2}^{h_i}\bar{u}_{h_2}$			106	F			21	23
$I_{h_3}^{h_i}\bar{u}_{h_3}$				F				22

TABLE 4.4
The number of global Newton iterations with different initial guesses (follower pressure load).

Method	IN				NEPIN			
Initial guess\Mesh	M_1	M_2	M_3	M_4	M_1	M_2	M_3	M_4
0	F	F	F	F	F	F	F	F
$I_{h_1}^{h_i}\bar{u}_{h_1}$	28	88	144	F	23	28	30	69
$I_{h_1}^{h_i}u_{h_1}$		87	97	F		20	21	F
$I_{h_2}^{h_i}u_{h_2}$			42	F			14	33
$I_{h_3}^{h_i}u_{h_3}$				F				17

TABLE 4.5
The performance of NEPIN using different tolerances δ and ρ_{res} (GN: the number of global Newton iterations; ANE: $\frac{\text{the total Newton iterations for NE}}{\text{the number of NE}}$; pct.: the maximum percentage of the eliminated equations).

Mesh		M_2			M_3			M_4		
δ \ ρ_{res}		0.7	0.8	0.9	0.7	0.8	0.9	0.7	0.8	0.9
0	GN	25	23	21	30	34	47	31	52	50
	ANE	$\frac{21}{10}$	$\frac{22}{14}$	$\frac{25}{17}$	$\frac{68}{17}$	$\frac{57}{29}$	$\frac{77}{42}$	$\frac{60}{26}$	$\frac{118}{47}$	$\frac{108}{45}$
	pct.	3.9%	4.4%	3.0%	3.3%	4.3%	0.8%	0.8%	0.5%	0.2%
1	GN	25	32	30	24	21	26	24	28	34
	ANE	$\frac{42}{5}$	$\frac{30}{4}$	$\frac{71}{10}$	$\frac{99}{12}$	$\frac{133}{12}$	$\frac{108}{21}$	$\frac{119}{16}$	$\frac{135}{22}$	$\frac{175}{26}$
	pct.	4.9%	4.9%	4.9%	4.0%	4.1%	4.1%	3.6%	1.9%	0.6%
2	GN	100	69	56	29	30	22	26	21	30
	ANE	$\frac{0}{0}$	$\frac{8}{1}$	$\frac{50}{3}$	$\frac{161}{13}$	$\frac{131}{12}$	$\frac{117}{12}$	$\frac{110}{12}$	$\frac{128}{14}$	$\frac{199}{23}$
	pct.	0%	4.5%	4.9%	4.4%	3.6%	4.8%	3.0%	2.7%	1.2%

factors impacting the performance of NEPIN: how to choose the equations to eliminate (which depends on the choice of δ and ρ_{res}) and how approximately the subproblems need to be solved (which depends on the choice of γ_a and γ_r). Next we investigate these two factors one by one based on the test example with simple pressure load.

First, we fix $\gamma_a = 1\text{e}{-6}$ and $\gamma_r = 1\text{e}{-1}$. The index set S_b^δ of the eliminated equations is determined by two tolerances ρ_{res} and δ. Table 4.5 lists the convergence results of NEPIN for different values of ρ_{res} and δ. In the middle row of the table, where $\delta = 1$, the performance of NEPIN is not sensitive to the choice of ρ_{res}. The number (GN) of global Newton iterations varies from 21 to 34, which indicates the convergence of NEPIN is almost uniform with respect to the mesh size. In the other rows of the table, the values of GN in the blocks of $(\delta = 0, M_4)$ and $(\delta = 2, M_2)$ vary drastically as ρ_{res} is changed. For the coarse mesh M_2, δ should not be larger than 1; otherwise the size of S_n^δ, i.e., the number of equations to eliminate, is larger than the threshold $n\rho_{size}$ and hence the NE step is skipped. For the fine mesh M_4, δ should be larger than 0; otherwise the preconditioning effect of NEPIN is too weak and hence the decrease of the residual is too slow.

TABLE 4.6
The performance of NEPIN using different tolerance γ_r for subproblems.

Mesh\γ_r	1e−1		1e−2		1e−4		one step	
	GN	ANE	GN	ANE	GN	ANE	GN	ANE
M_2	23	$\frac{25}{17}$	25	$\frac{80}{18}$	23	$\frac{66}{17}$	23	$\frac{21}{21}$
M_3	24	$\frac{121}{14}$	25	$\frac{203}{15}$	24	$\frac{251}{15}$	70	$\frac{44}{44}$
M_4	24	$\frac{180}{17}$	19	$\frac{202}{12}$	19	$\frac{301}{15}$	98	$\frac{82}{82}$

A satisfying observation from Table 4.5 is that the percentage (see the values of pct.) of the equations to eliminate decreases as the mesh is refined, which indicates that the size of the subproblems is not proportional to the size of the global problems. Another statistic in Table 4.5 is ANE, which stands for the average Newton iterations per NE step. The denominator of ANE is the number of NE steps applied during the global nonlinear iteration, while the numerator of ANE is the total Newton iterations for all the NE steps. The value of ANE increases if δ increases, which indicates that more computational cost is paid for enforcing the nonlinear preconditioning effect. For the recommended choice $\delta = 1$, the value of ANE is about 8 for all the testing meshes, but the number of NE steps increases a little bit.

Second, we fix $\delta = 1$, $\rho_{res} = 0.7$, and $\gamma_a = 1\text{e}{-6}$. Table 4.6 shows the performance of NEPIN for different γ_r. A very loose tolerance $\gamma_r = 1\text{e}{-1}$ is sufficient, which is the same as the results in [15]. Higher accuracy does not improve the convergence too much. However, only one step in the nonlinear iteration of NE is not enough. Note that it is always the relative tolerance γ_r that stops the nonlinear iteration of NE. If the residual is of magnitude $\gamma_a = 1\text{e}{-6}$, the quadratic convergence of Newton's method is observed for our test examples. That is why we do not expose the performance of NEPIN for different γ_a.

5. Conclusions. The main contribution of this paper is to present a detailed analysis of the preconditioning effect of NE and to apply the proposed method to three-dimensional heterogeneous hyperelastic problems. In theory, we prove that the exact NE is able to reduce the residual and the local Lipschitz constant of the nonlinear function and hence accelerates the convergence of the Newton method. For numerical computation, we propose a robust strategy to detect the equations causing the nonlinear stagnation. We also find two effective tricks to ease the thrashing phenomenon of NE: using an initial guess interpolated from a coarse level solution and extending the eliminating index set by adding the neighboring degrees of freedom. In future work, we will consider other arterial wall problems with patient-specific geometry and the parallel performance of the algorithm.

REFERENCES

[1] S. BALAY, S. ABHYANKAR, M. F. ADAMS, J. BROWN, P. BRUNE, K. BUSCHELMAN, L. DALCIN, V. EIJKHOUT, W. D. GROPP, D. KAUSHIK, M. G. KNEPLEY, L. C. MCINNES, K. RUPP, B. F. SMITH, S. ZAMPINI, H. ZHANG, AND H. ZHANG, *PETSc Users Manual*, Tech. Report ANL-95/11, Revision 3.7, Argonne National Laboratory, 2018.

[2] J. M. BALL, *Convexity conditions and existence theorems in nonlinear elasticity*, Arch. Ration. Mech. Anal., 63 (1976), pp. 337–403.

[3] D. BALZANI, S. DEPARIS, S. FAUSTEN, D. FORTI, A. HEINLEIN, A. KLAWONN, A. QUARTERONI, O. RHEINBACH, AND J. SCHRÖDER, *Numerical modeling of fluid–structure interaction in arteries with anisotropic polyconvex hyperelastic and anisotropic viscoelastic material models at finite strains*, Int. J. Numer. Methods Biomed. Eng., 32 (2016), e02756.

[4] D. Balzani, P. Neff, J. Schröder, and G. A. Holzapfel, *A polyconvex framework for soft biological tissues. Adjustment to experimental data*, Int. J. Solids Struct., 43 (2006), pp. 6052–6070.
[5] Y. Bazilevs, K. Takizawa, and T. E. Tezduyar, *Computational Fluid-Structure Interaction: Methods and Applications*, John Wiley & Sons, New York, 2013.
[6] D. Brands, A. Klawonn, O. Rheinbach, and J. Schröder, *Modelling and convergence in arterial wall simulations using a parallel FETI solution strategy*, Comput. Methods Biomech. Biomed. Eng., 11 (2008), pp. 569–583.
[7] X.-C. Cai and D. E. Keyes, *Nonlinearly preconditioned inexact Newton algorithms*, SIAM J. Sci. Comput., 24 (2002), pp. 183–200.
[8] X.-C. Cai and X. Li, *Inexact Newton methods with restricted additive Schwarz based nonlinear elimination for problems with high local nonlinearity*, SIAM J. Sci. Comput., 33 (2011), pp. 746–762.
[9] R. S. Dembo, S. C. Eisenstat, and T. Steihaug, *Inexact Newton methods*, SIAM J. Numer. Anal., 19 (1982), pp. 400–408.
[10] P. Deuflhard, *Newton Methods for Nonlinear Problems: Affine Invariance and Adaptive Algorithms*, Springer Ser. Comput. Math. 35, Springer, New York, 2011.
[11] S. C. Eisenstat and H. F. Walker, *Globally convergent inexact Newton methods*, SIAM J. Optim., 4 (1994), pp. 393–422.
[12] G. A. Holzapfel, *Determination of material models for arterial walls from uniaxial extension tests and histological structure*, J. Theoret. Biol., 238 (2006), pp. 290–302.
[13] G. A. Holzapfel, T. C. Gasser, and R. W. Ogden, *A new constitutive framework for arterial wall mechanics and a comparative study of material models*, J. Elasticity, 61 (2000), pp. 1–48.
[14] J. Huang, C. Yang, and X.-C. Cai, *A nonlinearly preconditioned inexact Newton algorithm for steady state lattice Boltzmann equations*, SIAM J. Sci. Comput., 38 (2016), pp. A1701–A1724.
[15] F.-N. Hwang, Y.-C. Su, and X.-C. Cai, *A parallel adaptive nonlinear elimination preconditioned inexact Newton method for transonic full potential equation*, Comput. Fluids, 110 (2015), pp. 96–107.
[16] A. Klawonn, M. Lanser, and O. Rheinbach, *Nonlinear FETI-DP and BDDC methods*, SIAM J. Sci. Comput., 36 (2014), pp. A737–A765.
[17] A. Klawonn, M. Lanser, and O. Rheinbach, *Toward extremely scalable nonlinear domain decomposition methods for elliptic partial differential equations*, SIAM J. Sci. Comput., 37 (2015), pp. C667–C696.
[18] A. Klawonn, M. Lanser, O. Rheinbach, and M. Uran, *Nonlinear FETI-DP and BDDC methods: A unified framework and parallel results*, SIAM J. Sci. Comput., 39 (2017), pp. C417–C451.
[19] P. Ciarlet, *Mathematical Elasticity, Vol.* I: *Three-Dimensional Elasticity*, Stud. Math. Appl. 20, North-Holland, Amsterdam, 1988.
[20] P. J. Lanzkron, D. J. Rose, and J. T. Wilkes, *An analysis of approximate nonlinear elimination*, SIAM J. Sci. Comput., 17 (1996), pp. 538–559.
[21] A. Logg, K.-A. Mardal, and G. Wells, *Automated Solution of Differential Equations by the Finite Element Method: The FEniCS Book*, Lect. Notes Comput. Sci. Eng. 84, Springer, New York, 2012.
[22] J. Schröder and P. Neff, *Invariant formulation of hyperelastic transverse isotropy based on polyconvex free energy functions*, Int. J. Solids Struct., 40 (2003), pp. 401–445.